Aptamer-Functionalized Multidimensional Conducting-Polymer Nanoparticles for an Ultrasensitive and Selective Field-Effect-Transistor Endocrine-Disruptor Sensors

*Jun Seop Lee, Sung Gun Kim, Jaemoon Jun, Dong Hoon Shin, and Jyongsik Jang**

An endocrine disruptor (ED) is a type of xenobiotic compound that can cause serious diseases related to the estrous cycle, as well as various types of cancer. At low ED concentrations, estrogen receptors may respond as they would under physiological conditions. In this work, aptamer-functionalized multidimensional conducting-polymer (3-carboxylate polypyrrole) nanoparticles (A_M_CPPyNPs) are fabricated for use in an FET sensor to detect bisphenol A (BPA). The multidimensional system, M_CPPyNPs, is first produced by means of dual-nozzle electrospray of pristine CPPyNPs and vapor deposition polymerization of additional conducting polymer. The M_CPPyNPs are then immobilized on an amine-functionalized ($-NH_2$) interdigitated-array electrode substrate, through the formation of covalent bonds with amide groups (–CONH). The amine-functionalized BPA-binding aptamer is then introduced in the same way as that for M_CPPyNP immobilization. The resulting A_M_CPPyNP-based FET sensors exhibit ultrasensitivity and selectivity towards BPA at unprecedentedly low concentrations (1 fM) and among molecules with similar structures. Additionally, due to the covalent bonding involved in the immobilization processes, a longer lifetime is expected for the FET sensor.

1. Introduction

Recently, xenobiotic compounds have been detected in large quantities in the human environment and in various chemical product fabrications.[1–4] One such type of xenobiotic compounds, endocrine disruptors (EDs), has a structure that is similar to estrogen. EDs show an affinity for human estrogen receptors (ERs), such as ER-α and ER-β, and have been linked to serious diseases related to the estrous cycle, such as male infertility and various types of cancer.[5–10] Among EDs, bisphenol A (BPA) has emerged as a particularly harmful material, due to its widespread use in the raw materials of plastics and its release from polycarbonate bottles at high temperatures.[11–14] ERs associated with the cell membrane can simulate physiological responses at low BPA concentrations (100 pM).[15–17] In addition to its association with infertility and cancer, BPA is also linked to cardiovascular disease and diabetes.[18–20] Therefore, the release of BPA from plastic packaging or cups should be accurately monitored on site for human health.

Several analytical methods have been examined for the detection of BPA at low concentrations.[21–24] Chromatographic techniques are commonly used for BPA detection. These include high-pressure liquid chromatography (HPLC) and gas chromatography coupled with mass spectrometry (GC-MS); however, these chromatographic techniques require sample pretreatment and complex equipment. Additionally, immunoassay-based methods have attracted considerable attention due to their high sensitivity for BPA and comparable low cost; however, because accurate BPA detection depends strongly on the quality of the prepared antibody and non-specific binding to analytes having a similar structure, these techniques are not used as frequently.

Nucleic acid aptamers, which are synthetic molecules of single-stranded DNA (ssDNA) or RNA, have been receiving significant attention since 1990.[25,26] Aptamers can detect small molecules, such as environmental pollutants, food toxicants, and disease-related metabolites in solution, through conformational changes after binding with a target.[27–30] Compared with antibodies, aptamers are better capture agents for small molecules, for the following reasons. First, their small structure more accurately discriminates between the functional groups of similar structures. Second, small molecules can be targeted in vitro, without the need for hapten, which is often required to facilitate the selection of antibodies among other molecules. Numerous studies have examined the applicability of aptamers to disease-state targeting.[31–33] Among a variety of aptamer-based detection techniques, electrochemical detection, which is based on redox reactions, exhibits rapid degradation over time.[34,35]

Conducting polymers (CPs)—e.g., polypyrrole (PPy), polyaniline (PANI), and polythiophene—exhibit interesting chemical and physical properties, due to their conjugated polymer backbone comprising alternating single and double bonds.[36] Due to their unique properties, CPs have been used as sensor transducers with inherent electronic, optical, and mechanical

J. S. Lee, S. G. Kim, J. Jun, D. H. Shin, Prof. J. Jang
School of Chemical and Biological Engineering
College of Engineering
Seoul National University
599 Gwanangno, Gwanakgu, Seoul 151–742, Korea
E-mail: jsjang@plaza.snu.ac.kr

DOI: 10.1002/adfm.201401166

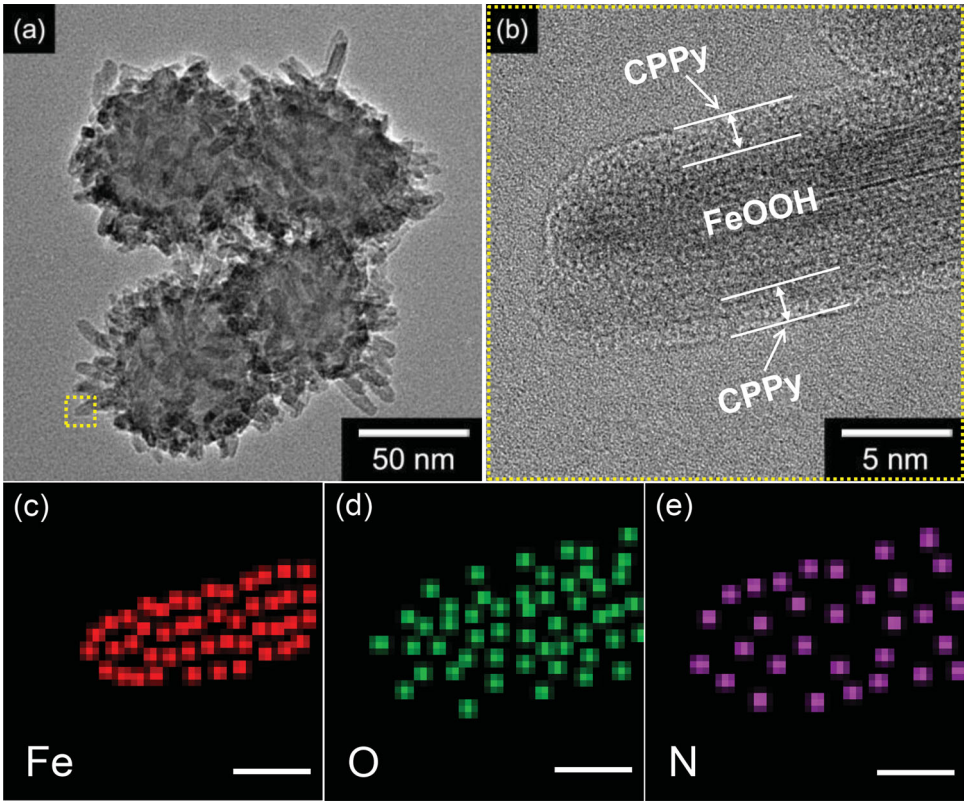

Figure 1. a) TEM image of multidimensional carboxylated polypyrrole nanoparticles (M_CPPyNPs) based on CPPyNPs that were originally 60 nm in diameter. b) HR-TEM image of the needle of M_CPPyNP that is outlined in a. c–e) Electron energy loss spectroscopy (EELS) dot mapping of a needle on the M_CPPyNP surface, showing the Fe (red; c), O (green; d), and N (purple; e) atoms. Scale bars of (c) to (e) = 5 nm.

transducer mechanisms.[37–39] To enhance sensitivity, considerable effort has focused on the fabrication of nanometer-scale CPs, due to their beneficial characteristics, such as their small size, high surface-to-volume ratio, and amplified signals.[40–42] Recently, several studies have focused on enlarging the surface area of CP nanomaterials to maximize interactions between the CP transducers and analytes. For example, tetragonal star-like PANI was fabricated using a hydrothermal synthetic method and applied to dopamine sensors.[43] 3D PANI-hydrogels were synthesized with a high surface area and used in glucose oxidase sensors.[44] However, sensor device fabrication of these materials at the nanoscale is difficult.

Herein, we describe the fabrication of a field-effect transistor (FET)-type aptamer sensor to detect the ED known as BPA; the sensor comprises multidimensional carboxylated polypyrrole nanoparticles (M_CPPyNPs) conjugated with a BPA-binding aptamer. The surface area of the M_CPPyNPs is four times larger than that of pristine CPPyNPs, due to the formation of nanoneedles on the pristine NPs. As a result, the interaction between the analyte and M_CPPyNP-based transducer was enhanced. To the best of our knowledge, this is the first experimental demonstration of an FET-type aptasensor using M_CPPyNPs as signal transducers. Binding M_CPPyNPs on the FET substrate and immobilizing the BPA-binding aptamer results in a strong affinity between the aptamer and BPA, thus providing an aptamer–FET platform suitable for electronic control. Field-induced sensitivities to various BPA concentrations were observed, eventually leading to the recognition of BPA at unprecedentedly low concentrations (1 fM). This FET-type aptasensor exhibited high selectivity to the target analyte (BPA) among molecules with a structure similar to BPA; in addition, its lifetime is relatively long compared with other biosensors.

2. Results and Discussion

2.1. Fabrication of M_CPPyNPs

Multidimensional 3-carboxylate polypyrrole nanoparticles (M_CPPyNPs) were fabricated using dual-nozzle electrospray and vapor deposition polymerization (VDP). As a starting material, pristine CPPyNPs (diameter: 30, 60, and 100 nm) were synthesized through chemical copolymerization of pyrrole and pyrrole-3-carboxylic acid using the dispersion method (molar ratio for (pyrrole):(pyrrole-3-carboxylic acid) = 30:1).[34,37] The pyrrole-3-carboxylic acid functional units were incorporated into the pyrrole repeating units through α–α' covalent linkages without any degradation to their dominant physical properties. The 3-carboxylate polypyrrole nanoparticles (CPPyNPs) were then mixed with an $FeCl_3$ aqueous solution as described in the following. The mixture was electrosprayed into an aqueous NaOH solution contained within a Petri dish; a dual-nozzle was used, in which the outer part sprayed the CPPyNP mixed

solution and the inner part compressed air.[45] The electrosprayed CPPyNPs were then mixed with the $FeCl_3$ aqueous solution at 70 °C for 4 h to induce growth of FeOOH needles on the surface of the CPPyNPs. The FeOOH-decorated hybrid CPPyNPs were then dipped into 5-wt% $CuCl_2$ ethanol solution. As a result, Cu cations adsorbed to the FeOOH needle surface, due to the charge–charge interaction between the Cu^{2+} ions and the partial negative charge of the oxygen atoms in the FeOOH structure (Supporting Information (SI): Figure S1). When the Cu cations were sufficiently adsorbed onto the FeOOH needles, a vaporized mixture of pyrrole and 3-carboxylated pyrrole monomers (molar ratio: 30:1) was allowed to copolymerize via chemical oxidation polymerization (i.e., VDP). As a result, a uniform CPPy layer (thickness: ca. 3 nm) formed on the surface, as confirmed by transmission electron microscopy (TEM) and high-resolution TEM (HRTEM) (**Figure 1**a,b). Electron energy loss spectroscopy (EELS) mapping of the Fe, O, and N atoms confirmed the composition of the CPPy-coated FeOOH needle surface following the VDP step (Figure 1c–e). The 30- and 100-nm CPPyNPs also formed a similar multidimensional morphology using the same process (SI: Figure S2). No aggregation of the coating particles was observed following polymerization, due to the uniform dispersion of the Cu cations on the FeOOH surfaces during adsorption. The surface area of the resulting M_CPPyNPs increased about fourfold, compared with pristine CPPyNPs; more specifically, the surface area increased from 100 to 396 $m^2\ g^{-1}$ for the 30-nm NPs, 50 to 204 $m^2\ g^{-1}$ for the 60-nm NPs, and 35 to 140 $m^2\ g^{-1}$ for the 100-nm NPs (**Figure 2**).

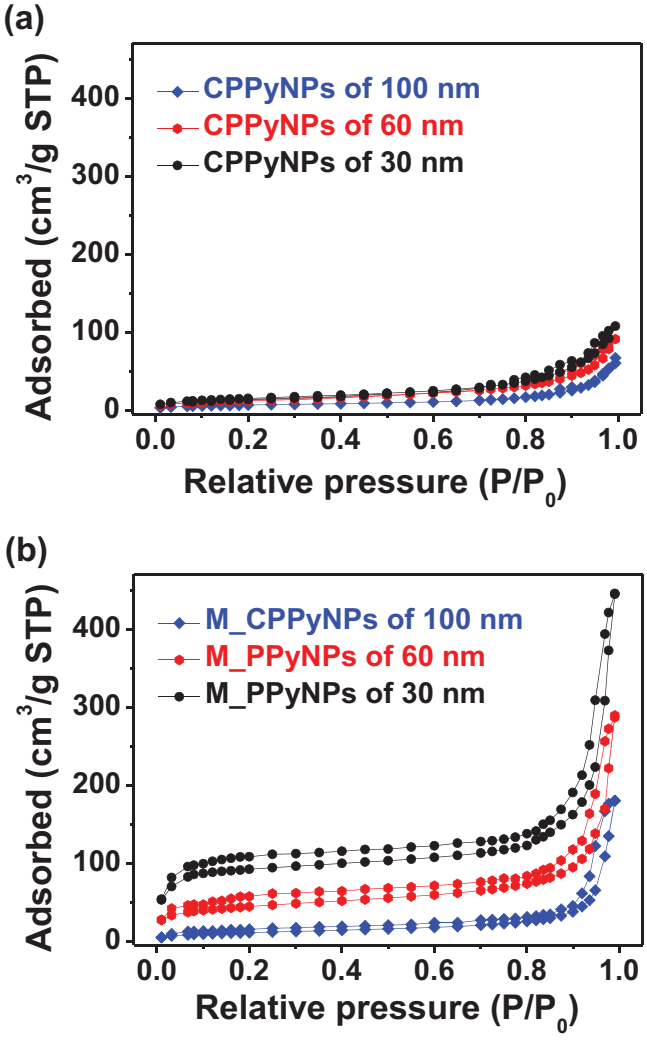

Figure 2. Nitrogen adsorption–desorption curves for a) pristine CPPyNPs with diameters of 30 (black), 60 (red), and 100 (blue) nm and b) the M_CPPyNPs resulting from CPPyNPs of those diameters. STP represents standard temperature and pressure.

2.2. Fabrication of Aptamer-Conjugated M-CPPyNP FET Sensor Electrodes

The stability of the sensing environment (i.e., the liquid-ion solution) and strong bonding between the transducer and binding receptors are critical factors in the fabrication of highly sensitive FET biosensor electrodes. To improve stability, the immobilization of the transducer on the sensor electrode and that of the binding receptor on the transducer were achieved via the covalent bonding of functional groups. **Figure 3** provides a schematic diagram of the procedure for the immobilization of the aptamer-conjugated M_CPPyNPs on the electrode substrate. An interdigitated microelectrode array (IDA) was patterned on a glass substrate using a lithographic process; the array was composed of pairs of gold electrode bands with 25 lines of fingers (SI: Figure S3). The IDA glass substrate was treated with 3-aminopropyltrimethoxysilane (APS) to functionalize the surface with amine groups ($–NH_2$). Subsequently, the M_CPPyNPs were anchored to the substrate through a condensation reaction between the carboxyl group (–COOH) of the NPs and the $–NH_2$ of the substrate involving the condensing agent 4-(4,6-dimethoxy-1,3,5-triazin-2-yl)-4-methylmorpholinium chloride (DMT-MM). The carboxyl group of the M_CPPyNPs facilitated the formation of a compact NP array on the substrate. In addition, the carboxyl group enabled the attachment of the binding aptamers to the particle surface. The 3′-end of the BPA-binding aptamer (see sequence in Experimental Section) was modified with a primary aliphatic amino linker for the covalent bonding between the BPA-binding aptamer and the carboxyl group of the M_CPPyNPs. A similar condensation reaction occurred between the amine group of the binding aptamer and the carboxyl group of the M_CPPyNPs. As a result, aptamer-conjugated M_CPPyNPs (A_M_CPPyNPs) were immobilized on the electrode substrate, and they demonstrated outstanding stability against environmental perturbation.

Figure 4a shows field-effect scanning electron microscopy (FE-SEM) images of the as-prepared immobilized A_M_CPPyNPs based on CPPyNPs of 60-nm diameter, with highly ordered packing on the IDA substrate. The arrays of ordered, packed hybrid NPs were clearly observed within the IDA. TEM images of the A_M_CPPyNPs indicated a rugged surface morphology and enlarged NPs, compared to M_CPPyNPs (i.e., there is evidence of aptamer conjugation) (Figure 4b). Additionally, when the hybrid NPs originating from the 30- and 100-nm CPPyNPs were packed on the IDA electrode in ordered array form, they showed a rugged surface morphology (SI: Figure S4) similar to that of the system from the 60-nm CPPyNPs.

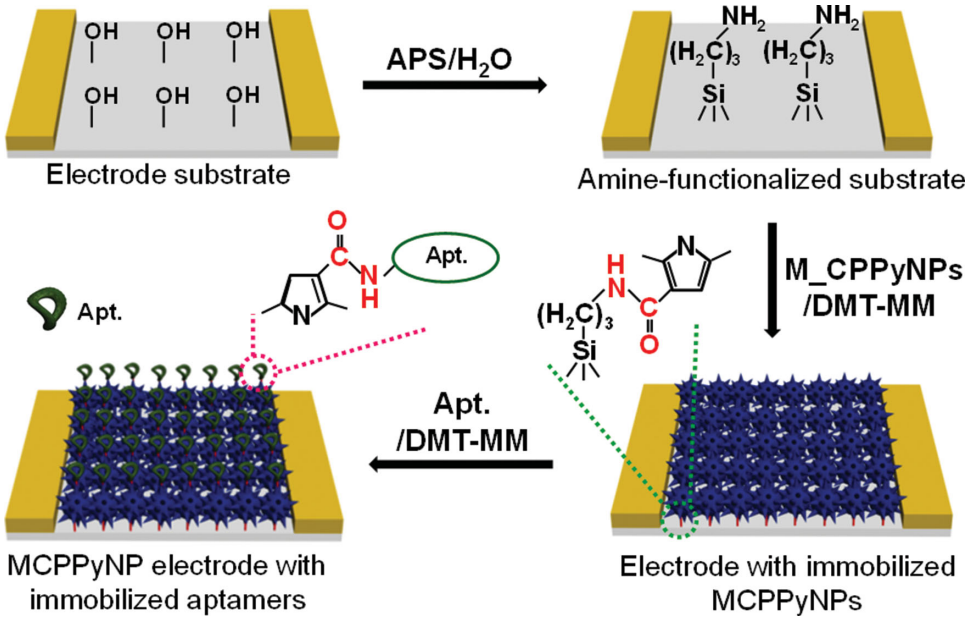

Figure 3. Schematic diagram of the immobilization process used to produce the sensor electrode based on aptamer-conjugated M_CPPyNPs (A_M_CPPyNPs) on the IDA electrode substrate. Apt. represents aptamer.

2.3. Characterization of Aptamer-Conjugated M-CPPyNP FET Sensor Electrodes

To characterize the electrical properties of the A_M_CPPyNPs in the liquid phase, an FET configuration was constructed using an electrolyte as a liquid-ion gate. Current–voltage (I–V) curves were used to evaluate the electrical contact of the A_M_CPPyNPs on the IDA substrate. **Figure 5**a shows the I–V characteristics of the M_CPPyNPs from the 30-, 60-, and 100-nm NPs, before and after immobilization of the BPA-binding aptamer. M_CPPyNPs with no aptamer conjugation exhibited linearity (i.e., ohmic contact) for voltages ranging from –0.1 to 0.1 V, as opposed to the nonlinearity exhibited by Schottky barriers with poor electrical contact at the electrode. The dI/dV values of the electrode increased, as the diameter of the M_CPPyNPs decreased, and decreased after the binding aptamer became immobilized on the particle surface. During aptamer introduction, the oxidation level of M_CPPyNP was changed owing to the detachment of doped element through condensation reaction. Nevertheless, linearity was maintained, and the dI/dV value was preserved with the same order of magnitude, after aptamer immobilization. Thus, these results suggest that the binding aptamers were effectively incorporated into the M_CPPyNPs, without any deterioration in electrical contact. Additionally, compared with pristine CPPyNPs, the electrical properties of the M_CPPyNPs exhibited higher conductivity, due to the enhanced contact area with the electrode substrate, arising from the presence of nanoneedles on the particle surface (Figure 5b).

Figure 6a shows a schematic diagram of the FET-sensor platform, based on A_M_CPPyNPs. Two gold IDA bands were used as the source (S) and drain (D) electrodes. The gate electrode was immersed in the electrolyte. The gate potential (V_G) was applied to the source electrode through a buffer solution. The distance between the electrodes was fixed at 2 mm, based on the resistivity of the buffer solution. To characterize the charge transport properties of A_M_CPPyNPs in the FET configuration, the dependence of the source–drain current (I_{SD}) with V_G variation (–20 to 100 mV) was investigated at a constant scan rate (10 mV s^{-1}) of source–drain voltage (V_{SD}). Figure 6b shows a plot of the I_{SD} versus V_{SD} for varying V_G, for A_M_CPPyNP electrode originating from 30-nm CPPyNPs. The I_{SD} increased negatively with negative enhancing V_G, indicating p-type (hole-transport) behavior, caused by an increase in the oxidation level of the polymer chains. The other A_M_CPPyNP electrodes (i.e., those made from 60- and 100-nm CPPyNPs) also exhibited p-type behavior (SI: Figure S5). Consequently, the dependence of I_{SD} on V_G confirmed that A_M_CPPyNP FETs could be effectively used as an electrochemical sensor for detecting analytes in solution. The liquid-ion gate is capable of achieving increased transconductance, due to the intimate contact between the NPs and the gate, compared with conventional backgating.

2.4. Real-Time Responses of Aptamer-Conjugated M-CPPyNP FET Sensor Electrodes

To investigate the sensing characteristics of the liquid-ion-gated A_M_CPPyNP FET, the I_{SD} was monitored in real time at a V_G of 10 mV (V_{SD} = 10 mV), a low operating voltage, upon the addition of various concentrations of BPA. **Figure 7**a shows the real-time response of the A_M_CPPyNP FET sensor originating from 30-, 60-, and 100-nm CPPyNPs as a function of BPA concentration. Upon each addition of BPA, the I_{SD} decreased rapidly over a 1-s period before reaching its saturated value. The decrease in I_{SD} may account for the intermolecular interaction that is induced in the formation of the aptamer–BPA complex. The carboxyl group in the polymer

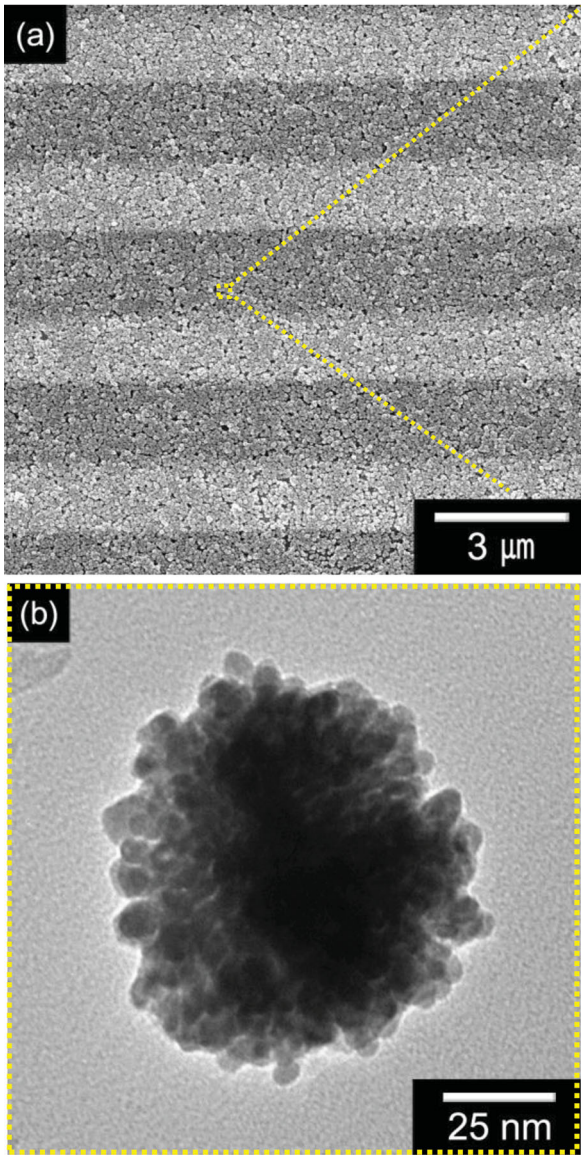

Figure 4. a) FE-SEM image of immobilized arrays of the BPA-binding A_M_CPPyNPs on the IDA substrate. b) TEM image of the BPA-binding A_ M_CPPyNP originating from 60-nm CPPyNPs.

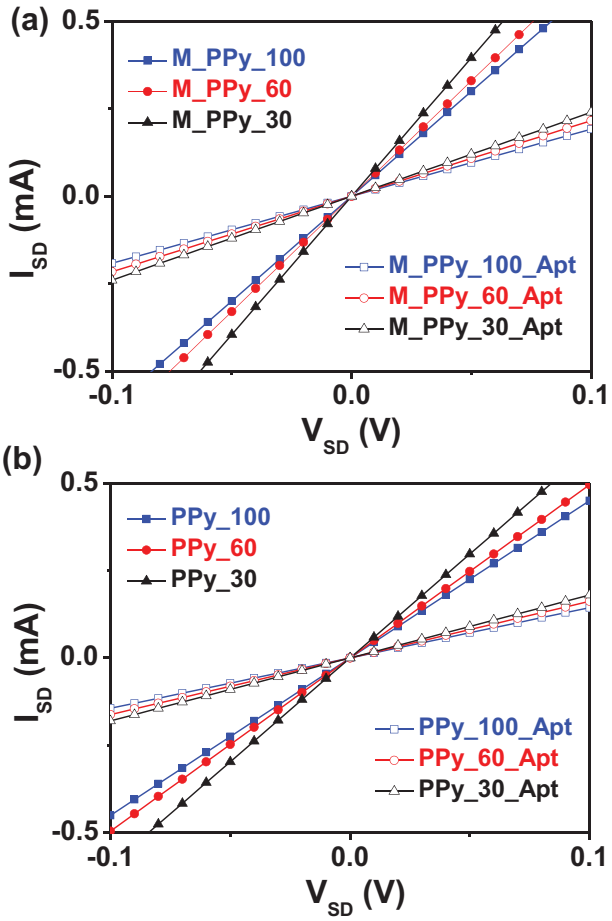

Figure 5. Source–drain current–voltage (I_{SD}–V_{SD}) curve comparison of the IDA electrodes based on a) the M_CPPyNPs and b) the CPPyNPs using CPPyNPs with a 30-, 60-, or 100-nm diameter, before and after the introduction of the BPA-binding aptamer (for a V_{SD} scan rate of 10 mV s^{-1}).

chains has a large dipole moment (μ = 2.6 D), and the BPA-binding aptamer has an overall negative charge.[34,46] Therefore, the BPA bonded to A_M_CPPyNPs can induce dipole–dipole or dipole–charge interactions between BPA and the aptamer-conjugated polymer chains. Particularly, the negative charge of the binding aptamers can be reduced by BPA molecules, when the BPA–aptamer complex forms. This intermolecular interaction reduces the hopping rate of charge carriers because 1) the Coulomb interaction between the positively charged polymer chains and counter ions becomes enhanced, and 2) a conformational change in the polymer chains is induced—from a linear form to a coil form. The sensitivity of the A_M_CPPyNP FETs increased as the NP diameter decreased; that is, the A_M_CPPyNP FET made from the 30-nm CPPyNPs was capable of detecting BPA concentrations as low as 1 fM at room temperature. The smaller-diameter NPs have a higher density of chemical functionality (degree of carboxylic acid group and aptamer introduced), compared with larger-diameter NPs; therefore, a better sensitivity was achieved with NPs originating from the 30-nm CPPyNPs as a result of the enhanced aptamer–BPA molecule interaction.

Figure 7b shows the changes in sensitivity as a function of NP diameter for the A_M_CPPyNPs, with respect to BPA concentration. The sensitivity (S) was determined from the saturation point of the normalized current change ($(\Delta I/I_0)_{SD} \times 100$), measured 10 s after the BPA addition. At low concentrations ($<10^0$ fM), the A_M_CPPyNP FET sensors showed nonlinear changes in sensitivity. In contrast, linear behavior was observed over a wide concentration range (10^0–10^4 fM). Compared with BPA sensors based on pristine CPPyNPs, the M_CPPyNPs presented a higher sensitivity of 10^2-fold (SI: Figure S6). Importantly, the sensitivity of the A_M_CPPyNP electrode originating from the 30-nm NPs was higher than that of the others, due to the enhancement of the active functional sites on its surface.

The selectivity of the A_M_CPPyNP FET towards the BPA molecule was investigated for several bisphenol molecules:

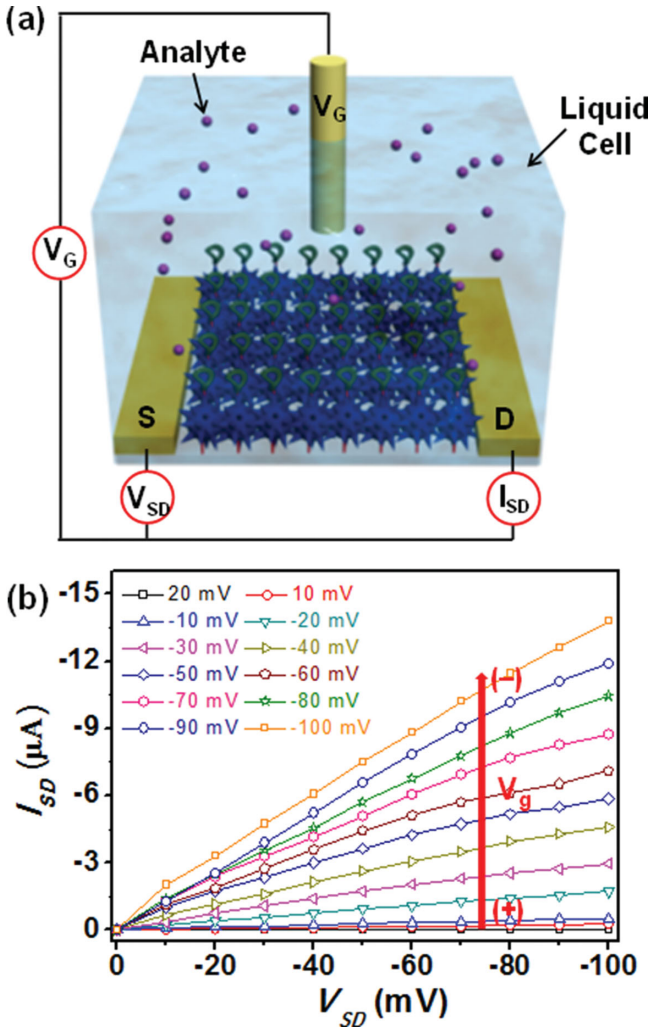

Figure 6. a) Schematic diagram of liquid-ion-gated FET with the A_M_CPPyNP array. b) Source–drain current versus source–drain voltage (I_{SD}–V_{SD}) characteristics of an A_M_CPPyNP FET electrode (in which the A_M_CPPyNPs originate from NPs of 30-nm diameter) for a varying gate voltage (V_G) ranging from 20 to −100 mV in −10 mV steps (V_{SD} scan rate: 10 mV s^{-1}).

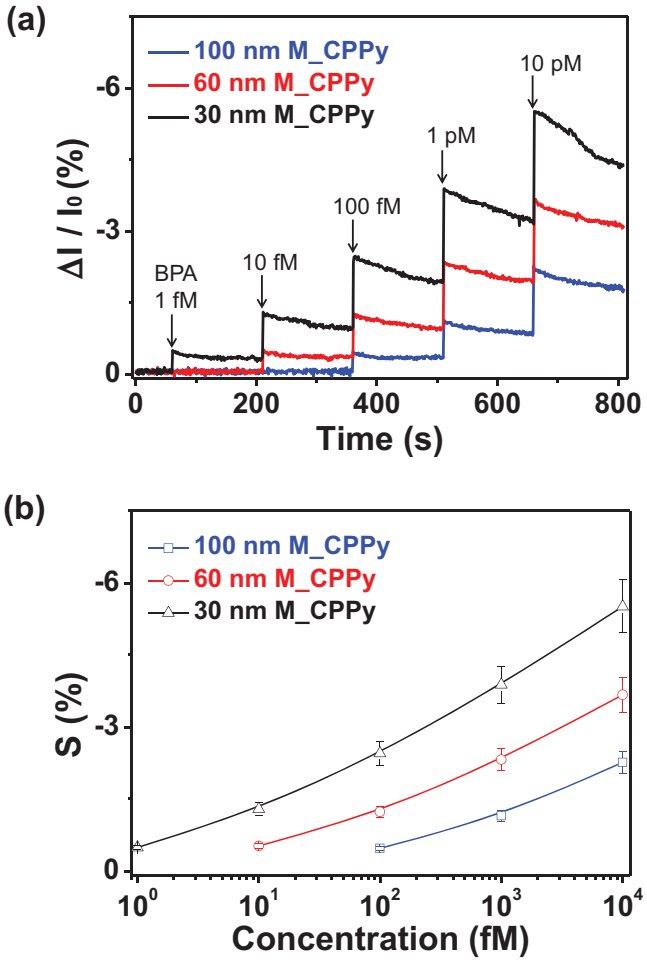

Figure 7. a) Real-time response for the FETs comprising various diameters of A_M_CPPyNP, with normalized current changes ($\Delta I/I_0 = (I - I_0)/I_0$, where I_0 is the initial current and I is the instantaneous current). b) Calibration curves of FETs comprising various diameters of A_M_CPPyNPs as a function of BPA concentration (S indicates the normalized current change after10 s of BPA exposure). Black, red, and blue represent FETs originatin from the 30-, 60-, and 100-nm CPPyNPs (V_G = 10 mV, V_{SD} = 10 mV).

bisphenol B (BPB), 4,4′-bisphenol (BP), 4,4-bis(4-hydroxyphenyl) valeric acid (VA), and 4,4′-(hexafluoroisopropylidene) diphenol (6F) (**Figure 8**). The A_M_CPPyNP sensor showed no significant I_{SD} changes with the addition of each 10 μM of non-target molecules; however, considerable I_{SD} changes were evident upon the addition of 1-fM BPA (Figure 8b). Additionally, to further confirm the selectivity of the FET sensors, real-time responses were conducted with the addition 10 μM non-target molecule mixtures; some of the mixtures contained 1 fM BPA, while other mixtures contained no BPA. Figure 8c shows significant signal changes after the addition of mixtures containing BPA, compared with the signal obtained for mixtures without BPA.

The main advantage of the chemical-bonding-based FET system is the repeated use (i.e., a longer lifetime); in contrast, adsorption-based systems that require washing/rinsing processes for re-use. **Figure 9** shows an estimation of the stability of the FETs based on A_M_CPPyNPs of various diameters over several weeks. To confirm stability, the A_M_CPPyNP FETs were stored in a sealed vessel at 25 °C for 4 weeks under air-dried conditions. The response of the A_M_CPPyNP FETs was displayed with 1 pM BPA concentration. Under these conditions, the S decreased to ca. 20% after 4 weeks (21%, 19%, and 18% for systems originating from the 30-, 60-, and 100-nm NPs, respectively). This decrease in sensitivity was attributed to the inactivation of the binding aptamer or the destruction of the nanoparticle array. However, the A_M_CPPyNP FETs maintained their other sensing abilities, such as selectivity and a minimum detectable level of BPA, despite the decrease in the response (SI: Figure S7).

3. Conclusion

We fabricated A_M_CPPyNP FET sensors using electrospray, VDP, and the introduction of a binding aptamer on the surface.

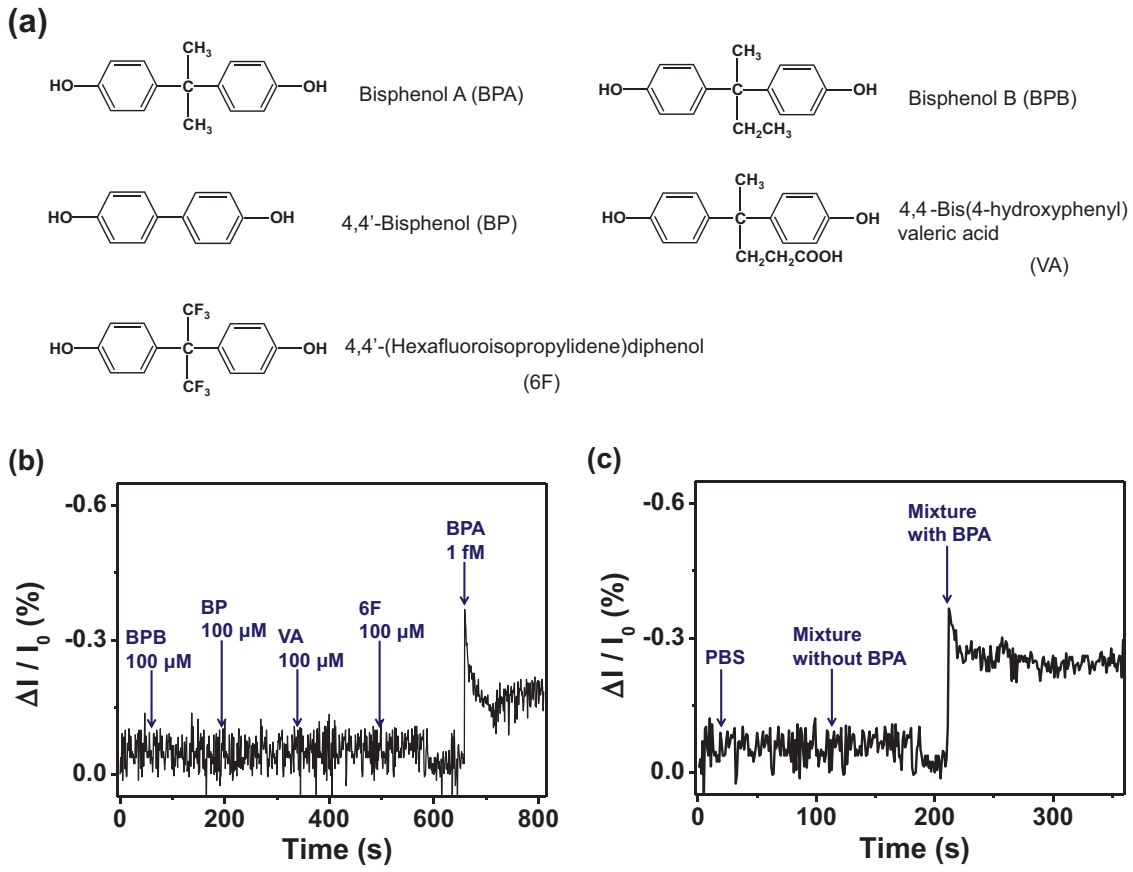

Figure 8. a) Molecular diagram of the bisphenol molecule family. b) Selectivity responses of the aptamer sensor using the A_M_CPPyNPs toward non-target (bisphenol B (BPB), 4,4′-bisphenol (BP), 4,4-bis(4-hydroxyphenyl) valeric acid (VA), and 4,4′-(hexafluoroisopropylidene) diphenol (6F)) and target (BPA) analytes. c) Real-time response of the aptamer sensor for various analytes, before and after being mixed with BPA (V_G = 10 mV, V_{SD} = 10 mV).

To our knowledge, this is the first demonstration of a multidimensional conducting-polymer nanoparticle-based FET-type aptamer sensor. The maximized surface area of the M_CPPyNPs enhanced the amount of conjugated BPA-binding aptamers, increasing its affinity for BPA. As a result, the A_M_CPPyNP FET sensors exhibited ultrahigh sensitivity (~1 fM) to BPA, 10–10^2 times higher than that of other FET sensors. Moreover, the A_M_CPPyNP sensor showed specific selectivity to the BPA molecule, as well as a long lifetime (4 weeks in this study) with respect to the repeated use of the sensor. The reusability properties of the sensor were attributed to the covalent bonding used in the immobilization process for sensing. Thus, this study demonstrates an effective method for fabricating FET sensors exhibiting ultrahigh sensitivity, using multidimensional conducting-polymer nanomaterials.

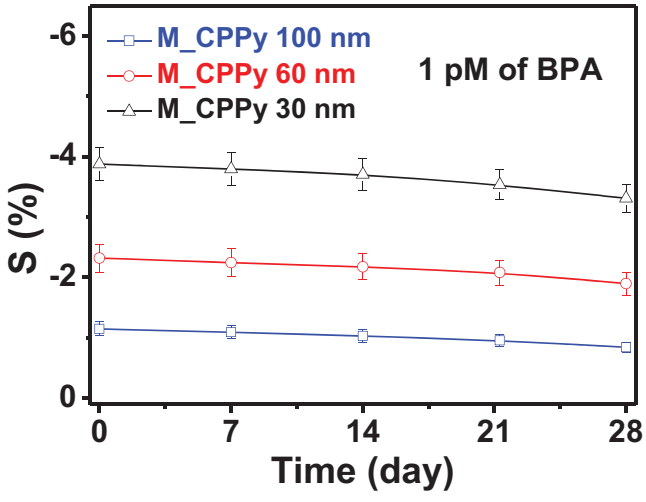

Figure 9. Comparison of the sensing performances of various A_M_CPPyNP-FET sensors undergoing 4 weeks of storage. Measurements were obtained at 1-week intervals. The A_M_CPPyNPs originated from CPPyNPs with 30- (black), 60- (red), and 100-nm (blue) diamters.

4. Experimental Section

Materials: Poly(vinyl alcohol) (PVA; molecular weight, MW: 9000), $FeCl_3$ (97%), and $CuCl_2$ (97%) were purchased from Aldrich Chemical Company and used without further purification. Pyrrole (98%) and pyrrole-3-carboxylic acid were purchased from Aldrich and Acros Organics. BPA (4,4′-(isopropylidene)diphenol), BPB (4,4′-(1-methylpropylidene)diphenol), VA, BP, and 6F were purchased from TCI. The BPA-binding aptamer was synthesized by Bioneer Co. (Daejeon, Korea); the sequence of the designed aptamer was 5′-NH_2-CCG GTG GGT GGT CAG GTG GGA TAG CGT TCC GCG TAT GGC CCA GCG CAT CAC GGG TTC GCA CCA-3′, where C, G, T, and A represent cytosine, guanine, thymine, and adenine, respectively. The

aptamer stock solution was diluted with diethyl pyrocarbonate (DEPC)-treated water and stored in the freezer before use (–20 °C).

Fabrication of M_CPPyNPs: Uniform CPPyNPs with diameters of 30, 60, and 100 nm were prepared with PVA, $FeCl_3$, and a mixture of pyrrole and pyrrole-3-carboxylic acid monomers (molar ratio of (pyrrole):(pyrrole-3-carboxylic acid) = 30:1), as described previously.[34,37] The CPPyNPs were electrosprayed along with compressed air through a dual nozzle at an applied voltage of 15 kV in to an aqueous NaOH solution contained within a Petri dish; the outer and inner parts of the spray were the CPPyNPs and air, respectively. The resulting aqueous solution of the electrosprayed CPPyNPs was dispersed in a 10-wt% $FeCl_3$ aqueous solution and then stirred for 4 h at 70 °C. The subsequent solution was then precipitated with ethanol several times and then dried at 70 °C for 12 h. The hybrid particles obtained were soaked in a 5-wt% $CuCl_2$ ethanol solution, and then exposed to a vaporized mixture of pyrrole and pyrrole-3-carboxylic acid monomers (molar ratio for (pyrrole):(pyrrole-3-carboxylic acid) = 30:1) for 5 min at room temperature in a vacuum chamber, to initiate VDP on the particle surface.

Fabrication of the A_M_CPPyNP FET Sensor: To construct the FET aptasensor, an IDA electrode was treated with 5-wt% aqueous aminosilane (APS) for 6 h to introduce amino groups to the electrode surface. The treated electrode was then exposed to a mixture of 0.1-wt% M_CPPyNP aqueous solution (40 μL) and 1-wt% DMT-MM aqueous solution (40 μL) for 12 h. Subsequently, the coupling reaction to attach the BPA-binding aptamer to the M_CPPyNP surface was carried out using a mixture of the binding aptamer and 1-wt% DMT-MM aqueous solution (40 μL) for 12 h. Afterward, the A_M_CPPyNP immobilized electrode was rinsed with distilled water and dried at room temperature.

Electrical Measurements of the A_M_CPPyNP FET Sensor: All electrical measurements were conducted using a Keithley 2612A source meter and probe station (MS TECH, Model 4000). To utilize the solution-based measurement, a solution chamber (volume: 200 μL) was designed and used. The change in the current was normalized as follows:

$$\left[\frac{\Delta I}{I_0}\right]_{SD}(\%) = \frac{(I - I_0)}{I_0} \times 100 \quad (1)$$

where I_0 represents the initial current, and I is the measured real-time current.

Instruments: TEM and HR-TEM images were obtained using JEOL JEM-200CX and JEOL JEM-3010 microscopes, respectively. A JEOL 6700 instrument was used to obtain FE-SEM images. Brunauer–Emmett–Teller (BET) surface areas were measured using an ASAP2010 (Micrometrics). EELS mapping of the hybrid nanoparticles was performed with a JEOL JEM 2100F.

Supporting Information

Supporting Information is available from the Wiley Online Library or from the author.

Acknowledgements

This research was supported by the National Research Foundation of Korea (NRF) grant funded by the Korea government (MEST) (no. 2011-0017125).

Received: April 11, 2014
Revised: May 17, 2014
Published online: July 31, 2014

[1] S. M. Rappaport, M. T. Smith, *Science* **2010**, *330*, 460.
[2] S. Boue, H. D. Leon, W. K. Schlage, M. J. Peck, H. Weiler, A. Berges, G. Vuillaume, F. Martin, B. Friedrichs, S. Lebrun, *Toxicology* **2013**, *314*, 112.
[3] A. F. Hernandez, F. Gil, M. Lacasana, M. Rodriguez-Barranco, A. Gomez-Martin, D. Lozano, A. Pla, *Food Chem. Toxicol.* **2013**, *61*, 164.
[4] D. E. Vidal-Dorsch, R. C. Colli-Dula, S. M. Bay, D. J. Greenstein, L. Wiborg, D. Petschauer, N. D. Denslow, *Environ. Sci. Technol.* **2013**, *47*, 11268.
[5] R. Chalasani, S. Vasudevan, *ACS Nano* **2013**, *7*, 4093.
[6] M. P. Leese, F. Jourdan, W. Dohle, M. R. Kimberley, M. P. Thomas, R. Bai, E. Hamel, E. Ferrandis, B. V. L. Potter, *ACS Med. Chem. Lett.* **2012**, *3*, 5.
[7] H. Kuang, H. Yin, L. Liu, L. Xu, W. Ma, C. Xu, *ACS Appl. Mater. Inter.* **2014**, *6*, 364.
[8] S. Hansen, C.-M. Lehr, U. F. Schaefer, *Adv. Drug Delivery Rev.* **2013**, *65*, 251.
[9] N. V. Tusar, D. Maucec, M. Rangus, I. Arcon, M. Mazaj, M. Cotman, A. Pintar, V. Kaucic, *Adv. Funct. Mater.* **2012**, *22*, 820.
[10] M. Yamada, K. Kato, K. Shindo, M. Namizu, M. Haruki, N. Sakairi, K. Ohkawa, H. Yamamoto, N. Noshi, *Biomaterials* **2001**, *22*, 3121–3126.
[11] A. Ballesteros-Gomez, S. Rubio, D. Perez-Bendito, *J. Chromatogr. A* **2009**, *1216*, 449.
[12] J.-H. Kang, F. Kondo, Y. Katayama, *Toxicology* **2006**, *226*, 79.
[13] H. H. Le, E. M. Carlson, J. P. Chua, S. M. Belcher, *Toxicol. Lett.* **2008**, *176*, 149.
[14] R. S. J. Alkasir, M. Ganesana, Y.-H. Won, L. Stanciu, S. Andreescu, *Biosens. Bioelectron.* **2010**, *26*, 43.
[15] W. Dekant, W. Volkel, *Toxicol. Appl. Pharm.* **2008**, *228*, 114.
[16] Z. Mei, H. Chu, W. Chen, F. Xue, J. Liu, H. Xu, R. Zhang, L. Zheng, *Biosens. Bioelectron.* **2013**, *39*, 26.
[17] S. Salian, T. Doshi, G. Vanage, *Reprod. Toxicol.* **2011**, *31*, 359.
[18] Z. C. Sanchez-Acevedo, J. Riu, F. X. Rius, *Biosens. Bioelectron.* **2009**, *24*, 2842.
[19] K. V. Ragavan, L. S. Selvakkumar, M. S. Thakur, *Chem. Commun.* **2013**, *49*, 5960.
[20] S. Jiao, J. Jun, L. Wang, *Talanta* **2014**, *122*, 140.
[21] M. Jo, J.-Y. Ahn, J. Lee, S. Lee, W. Hong, J.-W. Yoo, J. Kang, P. Dua, D.-K. Lee, S. Hong, S. Kim, *Oligonucleotides* **2011**, *21*, 85.
[22] K. Inoun, K. Kato, Y. Yoshimura, T. Makino, H. Nakazawa, *J. Chromatogr. B* **2000**, *749*, 17.
[23] Y. Watabe, T. Kondo, M. Morita, N. Tanaka, J. Haginaka, K. Hosoya, *J. Chromatogr. A* **2004**, *1032*, 45.
[24] N. Kuroda, Y. Kinoshita, Y. Sun, M. Wada, N. Kishikawa, K. Nakashima, T. Makino, H. Nakazawa, *J. Pharmaceut. Biomed.* **2003**, *30*, 1743.
[25] A. D. Ellington, J. W. Szostak, *Nature* **1990**, *346*, 818.
[26] C. Tuerk, L. Gold, *Science* **1990**, *249*, 505.
[27] O. S. Kwon, S. J. Park, J. Jang, *Biomaterials* **2010**, *31*, 4740.
[28] O. S. Kwon, S. J. Park, J.-Y. Hong, A.-R. Han, J. S. Lee, J. S. Lee, J. H. Oh, J. Jang, *ACS Nano* **2012**, *6*, 1486.
[29] J. H. An, S. J. Park, O. S. Kwon, J. Bae, J. Jang, *ACS Nano* **2013**, *7*, 10563.
[30] K. Muteryka, *Biosens. Bioelectron.* **2014**, *54*, 393.
[31] W. Song, R. L. Strack, N. Svensen, S. R. Jaffrey, *J. Am. Chem. Soc.* **2014**, *136*, 1198.
[32] L. Zhou, Z. Li, Z. Liu, J. Ren, X. Qu, *Small* **2013**, *9*, 4262.
[33] F. Liu, H. D. Ha, D. J. Han, T. S. Seo, *Small* **2013**, *9*, 3410.
[34] H. Yoon, J.-H. Kim, N. Lee, B.-G. Kim, J. Jang, *ChemBioChem* **2008**, *9*, 634.
[35] H. Yoon, J. Jang, *Adv. Funct. Mater.* **2008**, *19*, 1567.
[36] J. Jang, *Adv. Polym. Sci.* **2006**, *199*, 189–256.
[37] J.-Y. Hong, H. Yoon, J. Jang, *Small* **2010**, *6*, 679.
[38] J.-Y. Hong, S. O. Jeon, J. Jang, K. Song, S. H. Kim, *Org. Electron.* **2013**, *14*, 979.
[39] C. Duan, K. Zhang, C. Zhong, F. Huang, Y. Cao, *Chem. Soc. Rev.* **2013**, *42*, 9071.
[40] W.-K. Oh, O. S. Kwon, J. Jang, *Polym. Rev.* **2013**, *53*, 407.
[41] S. J. Park, O. S. Kwon, J. E. Lee, J. Jang, H. Yoon, *Sensors* **2014**, *14*, 3604.

[42] N. A. Kotov, J. O. Winter, I. P. Clements, E. Jan, B. P. Timko, S. Campidelli, A. Mazzatenta, C. M. Lieber, M. Prato, R. V. Bellamkonda, *Adv. Mater.* **2009**, *21*, 3970.
[43] E. Jin, X. Lu, X. Bian, L. Kong, W. Zhang, C. Wang, *J. Mater. Chem.* **2010**, *20*, 3079.
[44] L. Pan, G. Yu, D. Zhai, H. R. Lee, W. Zhao, N. Liu, H. Wang, B. Tee, Y. Shi, Y. Cui, *Proc. Natl. Acad. Sci. USA* **2012**, *109*, 9287.
[45] J. S. Lee, D. H. Shin, J. Jun, J. Jang, *ACS Nano* **2013**, *7*, 10139.
[46] R. Rezg, S. El-Fazaa, N. Gharbi, B. Mornagui, *Environ. Int.* **2014**, *64*, 83.